frontiers | Frontiers in Materials

ORIGINAL RESEARCH
published: 08 April 2022
doi: 10.3389/fmats.2022.796730

Effect of Multi-Source Ultrasonic on the Microstructure and Mechanical Properties of a Large Scale 2219 Al Alloy Ingot During Casting

Anqing Li[1,2], *Ripeng Jiang*[1,2]*, *Zhilin Liu*[1,2]*, *Ruiqing Li*[1,2] *and Yun Zhang*[2,3]

[1]Light Alloy Research Institutes, Central South University, Changsha, China, [2]State Key Laboratory of High Performance Complex Manufacturing, Changsha, China, [3]College of Mechanical and Electrical Engineering, Central South University, Changsha, China

Usage of high-energy ultrasonic vibration is an effective approach that can dramatically improve the performance of large-scale ingots. In this work, it was applied to manufacture large 2219 aluminum alloy ingots (630 mm in diameter and 4,500 mm in length). The degassing efficiency, the average size of α-Al grains, the morphology of the Al_2Cu phase under double-source ultrasound (DSU), and three-source ultrasound (TSU) were compared. Meanwhile, the influence of the ultrasonic field on the macroscopic segregation of the Cu content and mechanical properties was scientifically investigated. It was found that the degassing efficiency of TSU was significantly higher than that of DSU. The results also indicated that α-Al grains were effectively refined under the TSU technology from the center to the edge of the ingot. Additionally, the distribution of the macroscopic Cu content was more uniform, and the area fraction of the Al_2Cu phase was evidently decreased. The mechanical properties of the ingot were superior to samples with DSU technology. Furthermore, it was demonstrated that the stress concentration of the coarse Al_2Cu phase at the center of the DSU process led to the deterioration of the mechanical properties.

Keywords: high-energy ultrasonic, α-Al grains, Al_2cu phase, macroscopic segregation, mechanical properties

OPEN ACCESS

Edited by:
Xincun Zhuang,
Shanghai Jiao Tong University, China

Reviewed by:
Qiang Wang,
Wuhan University of Science and Technology, China
Dashan Sui,
Shanghai Jiao Tong University, China

***Correspondence:**
Ripeng Jiang
jiangripeng@163.com
Zhilin Liu
zhinlin.liu@csu.edu.cn

Specialty section:
This article was submitted to Mechanics of Materials, a section of the journal Frontiers in Materials

Received: *17 October 2021*
Accepted: *18 February 2022*
Published: *08 April 2022*

Citation:
Li A, Jiang R, Liu Z, Li R and Zhang Y (2022) Effect of Multi-Source Ultrasonic on the Microstructure and Mechanical Properties of a Large Scale 2219 Al Alloy Ingot During Casting. Front. Mater. 9:796730. doi: 10.3389/fmats.2022.796730

INTRODUCTION

2219 aluminum alloy, with excellent process performance, high specific strength, corrosion resistance, and sound weldability performance, is widely used for metal-skinned large aircraft and fuel tanks and plays a key role in the manufacturing of new generation aviation structural parts (Zhang et al., 2019c). First, it was cast into a large ingot. Then, the aluminum alloy ingot is subjected to a series of other processes, including homogenization, forging, and reaming, before finally, being used in aerospace or transportation industries (Liu Z. et al., 2019; Zhang et al., 2019a). However, due to thermal convection, thermal stress, and large temperature gradient, the solidification process of large aluminum alloy ingots is so complex and results in an uneven microstructure and solute distribution, serious cracking, and macrosegregation. Therefore, advanced casting technology is of great significance for the preparation of aluminum alloy round ingots with excellent properties (Zhang et al., 2019b). Some solutions were proposed to solve these problems, such as adding grain refiner, mechanical agitation, electromagnetic stirring, and ultrasonic field melt treatment technology (Liew et al., 2014; Kotadia et al., 2017). However, the addition of fine-grain agents would affect the composition of large-scale ingots, and electromagnetic stirring may bring potential

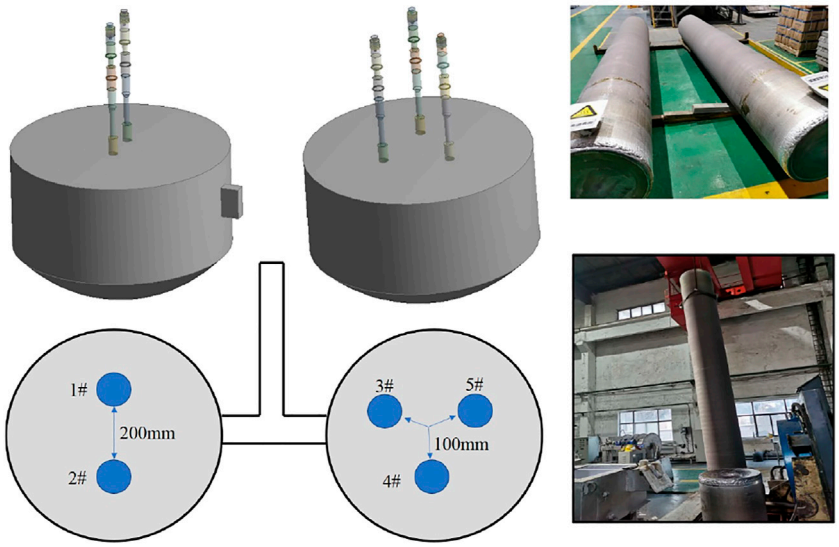

FIGURE 1 | Casting process diagram.

safety hazards. Therefore, the preparation of large-scale 2219 aluminum alloy ingots with excellent properties is still a great challenge (Zhang et al., 2019).

Usage of high-energy ultrasonic vibration has been proved to have great advantages in refining grains, reducing component segregation, and improving the machinability of ingots. Over the last few decades, many researchers have investigated the effect of single ultrasonic treatment on solidification (Zhang et al., 2011; Patel et al., 2012; Wang et al., 2017; Chen et al., 2018). Eskin et al. (Eskin and Eskin, 2003) found that ultrasonic treatment generated favorable merits, such as grain refinement, degassing, increasing solute solubility, and reducing segregation during alloy solidification. Jiang et al. (2014) studied the mechanism of ultrasonic vibration in 7,050 aluminum alloys and found that ultrasonic vibration could increase the solidification rate of the ingot. Chen et al. (2019) applied frequency conversion ultrasonic-assisted technology in the semi-continuous casting of AZ80 magnesium alloys, significantly promoted the heterogeneous nucleation, and reduced the grain size from 679–1,454 μm to 150–241 μm. Zhang et al. (Zhang et al., 2019b) introduced ultrasonic vibrations to Al-6.2 wt% Cu alloys. They found that almost all of the α-Al grains were transformed into equiaxed grains in the sample with 10-min continuous ultrasonic treatment. The aforementioned results indicate that the ultrasonic treatment has a positive effect on the refinement of inter-metallics and the improvement of the mechanical properties.

However, most of the previous studies focus on the microstructure and properties of small-size aluminum alloy ingots under the effect of single-power ultrasound. At the same time, the comparison of multi-source ultrasonic casting experiments is still rare. Regarding those large-scale casting (the diameter of ingots exceeds 550 mm), single ultrasonic treatment cannot induce satisfying results. In this article, double-source ultrasound (DSU) and three-source ultrasound (TSU) were applied during the solidification of large-scale 2219 Al ingots, respectively. Through introducing DSU and TSU, the microstructures and solute macro-segregation of the large-scale ingots were investigated. In addition, the mechanical properties of the two ingots were also tested and compared.

EXPERIMENT

Casting Procedures

A double-channel casting system was adopted in the casting platform. The schematic diagram of this experiment is shown in **Figure 1**. The unipolar ultrasonic system was independently designed with a maximum output power of 2 kW, a piezoelectric ceramic transducer of 20 kHz, a power cabinet, an air-cooled system, an ultrasonic transmitter, and a titanium alloy ultrasonic probe with a diameter of 50 mm. Each ultrasound system works independently. Before being inserted, the ultrasonic sonotrodes were preheated to improve the uniformity of the temperature field of the aluminum melt and avoid the chilling effect of ultrasonic. Second, ultrasonic sonotrodes were adjusted to a steady state to ensure vibration stability. During the casting process, ultrasonic sonotrodes were inserted into the liquid interface below 200 mm. According to a previous research study, the ultrasonic sonotrodes, which were at a depth of 200 mm, can play a better role in grain refinement and inhibiting the macroscopic segregation of components (Jiang et al., 2014). Before casting, the material was melted in an argon-protected melting system, followed by slagging, stirring, filtering and degassing, online testing of the alloy composition, and refining. Then, the molten aluminum alloy was poured into the double-channel casting system *via* the flow tank. After completing the aforementioned steps, the ultrasonic-assisted casting system was operated. The cooling water flowed around the crystallizer in the mold to solidify the ingot. At the same time,

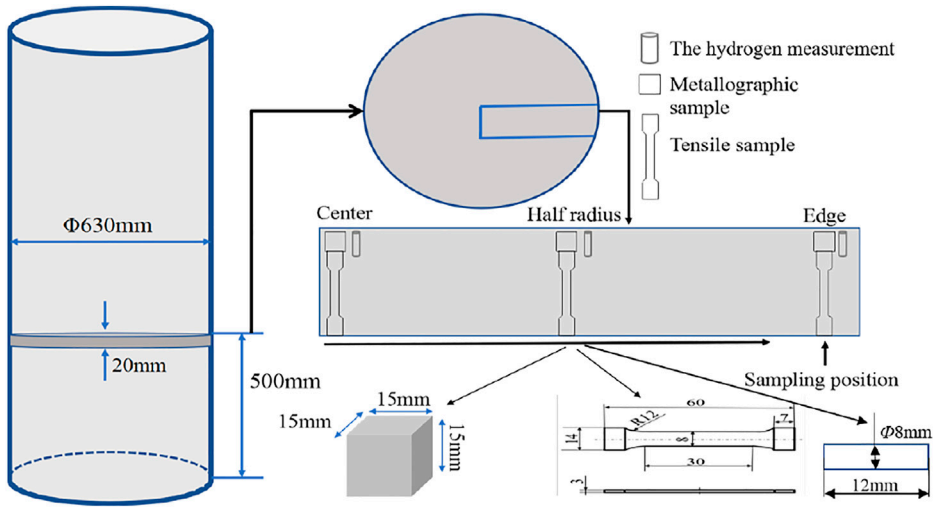

FIGURE 2 | Dimensions and sampling locations of the two ingots.

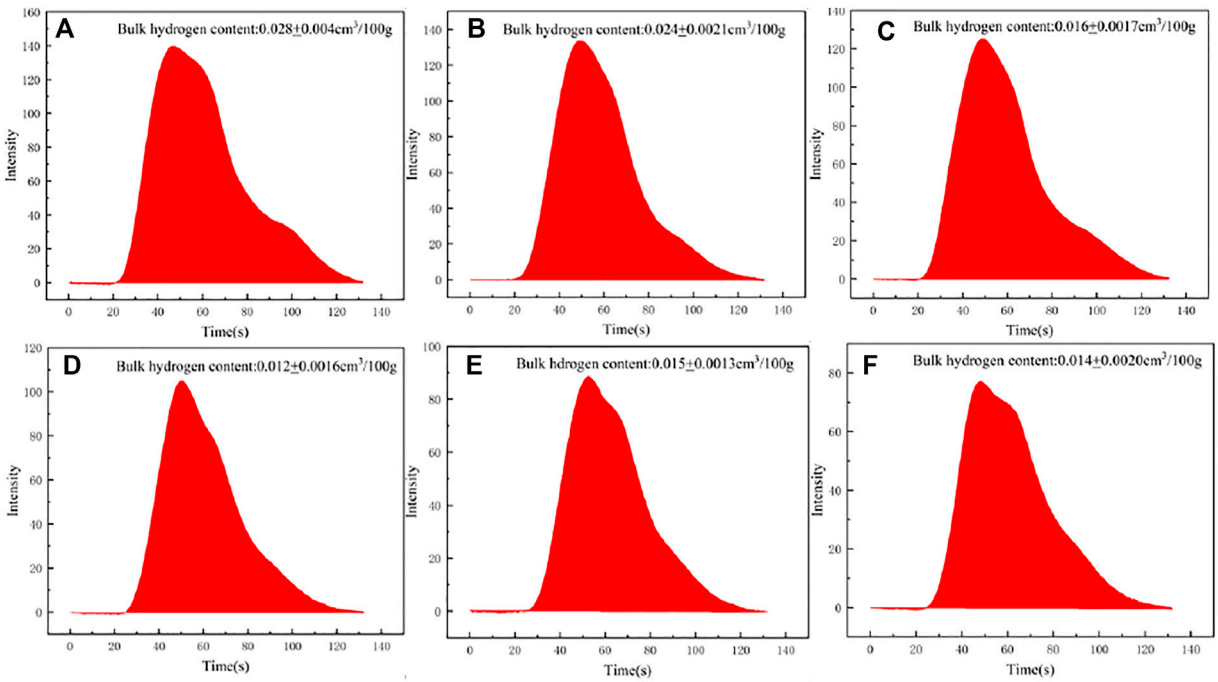

FIGURE 3 | Hydrogen content detection curves of **(A)** the center of DSU-treated ingot, **(B)** the half-radius of DSU-treated ingot, **(C)** the edge of DSU-treated ingot, **(D)** the center of TSU-treated ingot, **(E)** the half-radius of TSU-treated ingot, and **(F)** the edge of TSU-treated ingot.

water jets were continuously sprayed onto the surface of the ingot until the solidification was completed (Jiang et al., 2015; Li et al., 2016). There was a cylindrical hot-top applied to minimize the shrinkage involved. The output of each ultrasonic system was 600 ± 50 W, and the casting length was 4,500 mm. The casting was completed after about 4.5 h. Then, the two ingots with DSU and TSU were prepared for homogenization and comparison.

Characterization

After homogenization annealing, strip specimens, with a thickness of 20 mm and a length from the center to the edge, were taken from a distance of 5 00 mm away from the head of the two ingots. At the same time, metallographic samples of 15 mm × 15 mm × 15 mm and tensile samples were taken from the ingots, as shown in **Figure 2**. The RHEN600 Hydrogen determinator

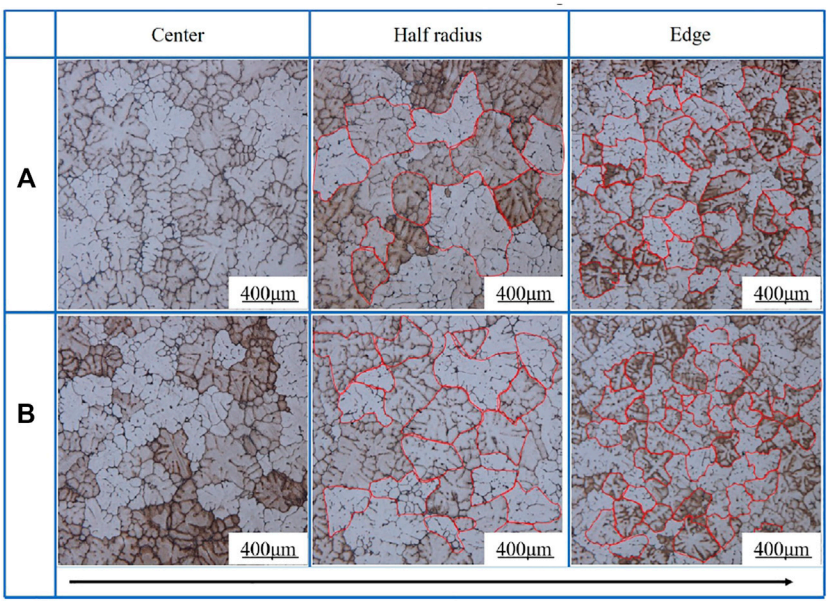

FIGURE 4 | Optical micrographs at the central and half-radial regions and the edge of the ingots treated with **(A)** DSU and **(B)** TSU.

(LECO Corporation, United States) was used to measure the hydrogen content of the sample to quantify the degassing efficiency of the ultrasonic field. The metallographic samples were mechanically grounded, polished, and etched using the standard metallographic technology (Wang F. et al., 2016). The metallography detection was conducted under polarized light by a ZEISS optical microscope. The grain size was analyzed by IPP 6 (Image-Pro Plus) software following a linear intercept method (ASTM112-10). The statistical analysis was conducted on the measured data. The mechanical properties were tested on an Instron 3,369 mechanical testing machine with a loading rate of 2mm/min.

RESULTS AND DISCUSSION

Hydrogen Content

Figure 3 shows the hydrogen content at each position of the ingot detected by the solid-state hydrogen meter. The hydrogen content in three positions of the ingot with DSU was 0.028 cm^3/100 g, 0.026 cm^3/100 g, and 0.016 cm^3/100 g, respectively. After applying TSU, it sharply decreased to 0.012 cm^3/100 g, 0.015 cm^3/100 g, and 0.014 cm^3/100 g, respectively. The degassing efficiency of TSU was increased by 57.1, 42.3, and 12.5%, respectively, compared with the DSU-treated ingot. Besides, the degassing efficiency at the center of the ingot of TSU was the highest, with a relative increase of 57.1%, and the degassing phase rate at the edge relatively increased by 12.5%. The solidification speed of ultrasonic ingots at the center was so slow that the hydrogen adsorbed in the aluminum melt was difficult to precipitate. The result showed that ultrasonic vibration played a significant role in the degassing process. At the edge position, due to the effect of cooling water, the solidification rate of the ingot with an increasing heat transfer rate was significantly higher than that at the center. Therefore, the precipitation rate of the hydrogen system was faster and less affected by ultrasonic vibration.

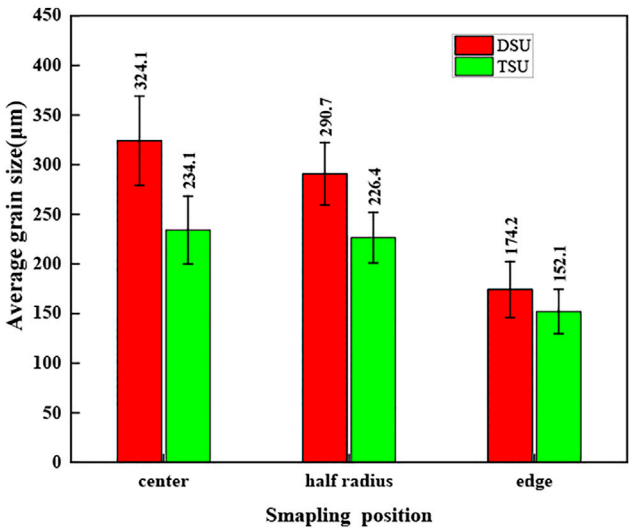

FIGURE 5 | The average grain size of α-Al grains at the representative positions of the ingots treated with DSU and TSU.

According to a previous research study (Xu et al., 2008; Eskin and Eskin, 2014), ultrasonic waves always produce cavitation and acoustic streaming effect during the alloy solidification process. Hollow bubbles expanded and compressed continuously under the cavitation effects and constantly adsorbed the surrounding

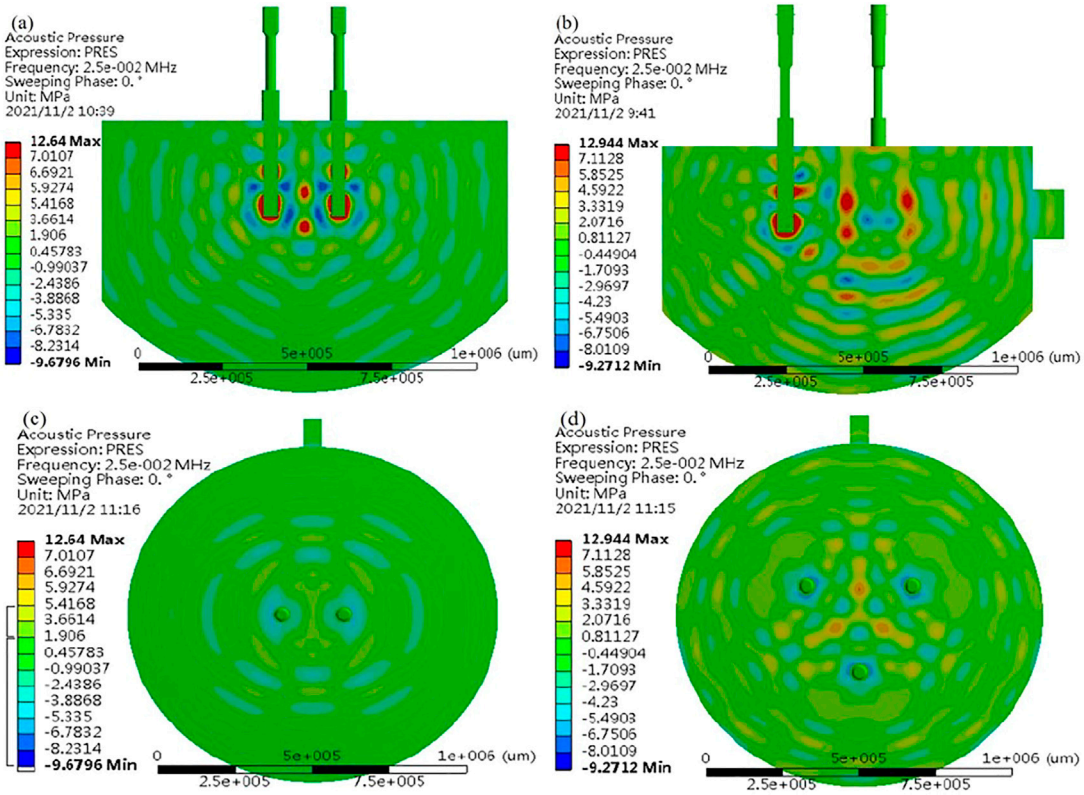

FIGURE 6 | Sound pressure simulation distribution diagram: **(A)** sound pressure distribution of the DSU-treated ingot, **(B)** sound pressure distribution of the TSU-treated ingot, **(C)** the top view of the DSU-treated ingot, and **(D)** the top view of the TSU-treated ingot.

gas to realize the continuous growth of the bubble. At the same time, under the effect of the acoustic streaming, they were discharged for the aluminum melt to realize the effect of degassing. Additionally, the growth of cavitation bubbles was further accelerated under the TSU treatment, resulting in a higher degassing efficiency than that with DSU. The previous result (Zhang et al., 2019c) has indicated that high-energy ultrasound can efficiently accelerate the heat transfer rate of aluminum melt and promote the precipitation rate of cavitation bubbles.

Microstructure of Primary α-Al Grains

The microstructures of the two ingots from different positions are shown in **Figure 4**. As can be seen from **Figure 4**, the size of the α-Al grains decreased gradually from the center to the edge. A lot of thick dendritic crystals were distributed in the central specimen, while in the half-radius and edge position, there were mostly equiaxed crystals. The half-radius part of TSU shows the equiaxed grain morphology, which is significantly different from DSU. To further demonstrate the difference of grains from the three parts, the grain size was measured by IPP 6.0 software. **Figure 5** shows the average grain size of the α-Al from the two ingots. The average grain size of the three positions of the ingot with DSU was 324.1, 290.7, and 174.2 μm, respectively. It decreased to 234.1, 226.4, and 152.1 μm, respectively, in TSU. The grain size of the center was slightly larger than that of the half-radius parts. In contrast to the ingot of DSU, the grain size is decreased by 27.8, 22.1, and 12.7%. The obvious difference in the grain size between two ingots indicated that the cavitation and acoustic streaming have a significant grain refinement effect on the α-Al (Sharma et al., 2009; Khosro Aghayani and Niroumand, 2011; Jiang et al., 2015; Li et al., 2016; Liu Y. et al., 2019).

Tiny cavitation bubbles were generated under the ultrasonic cavitation effect (Wang H. et al., 2016). Generally, they grow up in a very short time and eventually collapse under sound pressure, resulting in a local high pressure, which breaks the primary dendrites and increases nucleation sites (Liu Z. et al., 2019). Under the negative effect of ultrasonic cross pressure, the microjet produced by the cavitation bubble can clean the grain surface, break the dendrites, add new nucleation sites, and increase the wettability between grains (Jung et al., 2017). The simulation diagram of the acoustic pressure distribution of DSU and TSU-treated ingots is shown in **Figure 6**. The simulation process of the acoustic pressure field was carried out by Ansys 16.0. In the simulation model, the ultrasonic rod was inserted into the molten alloy with a depth of 200 mm and 100 mm away from the center. The finite element model took into account the coupling effects between the piezoelectric transducer, the acoustic pressure, the ultrasonic sonotrodes, and melts. The key parameters in the finite element model are shown in **Table 1**. The simulation results show that the superposition of DSU and TSU in the center led to a larger sound pressure value, which enhanced the center part's

TABLE 1 | Key parameters in the simulation model (Tian et al., 2018).

Materials	Elastic modulus (GPa)	density(kg.m^{-3}.10^{3})	Poisson's ratio
Piezoelectric ceramics	9.04	7.64	
Ultrasonic sonotrode	9.8	4.5	0.36
Alloy melt		2.45	0.35

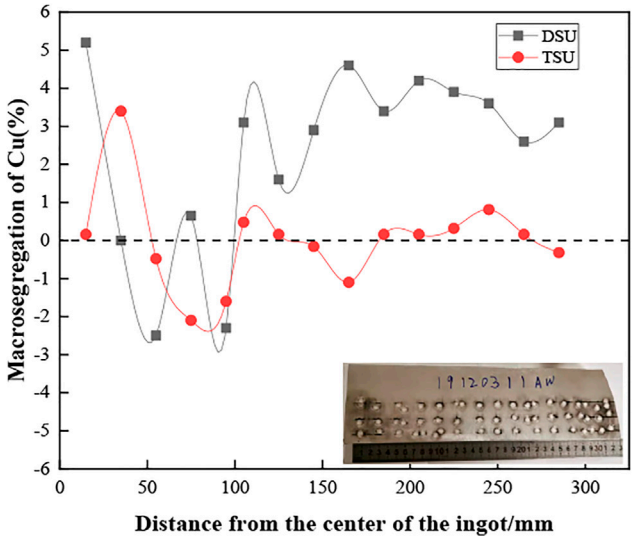

FIGURE 7 | Segregation curve of Cu solute elements.

nuclear and crushing nuclear capacities, and increased the number of nucleation particles (Ma et al., 2017; Moussa et al., 2018; Liu et al., 2019). As the new effective nucleation sites, compounds with high melting points in the aluminum melt, such as Al_3Ti (Wang et al., 2021) and BTi_2, can be uniformly distributed under the acoustic streaming effect of the ultrasonic field. Thus, more effective nucleation sites were activated, obviously increasing the nucleation rate (Wang H. et al., 2016). Acoustic streaming was also conducive to the uniform stability of the temperature gradient, and a great number of equiaxial crystals were formed during solidification (Jung et al., 2017). At the same time, the perturbation effect of the acoustic streaming effect was also higher than that of other positions. As the heat transfer and slow cooling rate weakened, more smaller grains were generated in the ingot than that in the ingot without ultrasonic application. This result is consistent with existing literature (Zhang et al., 2011; Wang H. et al., 2016).

The grain size of the DSU-treated ingot was decreased by 11.5% from the center to the edge. However, it was only 3.4% in the TSU-treated ingot. This also confirmed that ultrasonic vibration produced a more uniform heat transfer effect and a higher cooling rate. The grain size at the center of the ingot that underwent DSU treatment was larger than that of the center of the ingot that underwent TSU treatment. In general, the distribution area fraction of high pressure under the effect of TSU was larger than that under the effect of DSU, which also proved that the TSU had a better effect on the solidification structure of the ingot.

Change of Cu Content

Figure 7 shows the relative segregation curve of the Cu content from the center to the edge of the two different ingots. A direct reading spectrometer was used to detect samples along the radial direction on the transversal surface of ingots. The calculation formula is as follows (Li et al., 2016):

$$w = \frac{C_i - C_0}{C_i} \times 100\%. \quad (1)$$

Here, Ci is the Cu content at this position, C_0 is the average Cu content, and w is the relative segregation rate. The samples were tested every 20 mm for a set of data. Each set of data was measured at 3 points, and an average value was taken. Each sample was tested for 15 sets. The maximum positive segregation rate was 5.2%, and the maximum negative segregation rate was 2.5% in the DSU-treated ingot. They were 3.4 and 2.1%, respectively, in the TSU-treated ingot. It can be seen from **Figure 6** that the relative segregation rate of the ingot with DSU fluctuated considerably, and the distribution of the Cu content was also unstable. The maximum difference between the positive and negative relative segregation rates was 7.7%. The relative segregation rate distribution of the ingot with the TSU was relatively stable. The data was mostly concentrated around zero, and the maximum difference of positive and negative relative segregation rates was 5.5%, which confirms the relatively desired effect of controlled segregation and could meet the requirements for industrial production. In general, the distribution of the Cu content in the ingot with the DSU field fluctuated considerably with a poor uniformity, while the content of Cu in the sample in the TSU group was relatively stable. Compared with the DSU-treated ingot, the ingot treated with the TSU achieved an ideal industrial production effect.

During the solidification process of aluminum alloys, the solute distribution coefficient K_0 of Cu, Mg, Mn, and other elements was less than one. A large number of solute elements were precipitated from the matrix during the redistribution process. The results show that the actual partition coefficient of the aluminum alloy was affected by the solidification environment. The effective solute distribution coefficient K_e is defined as follows (Aziz, 1982):

$$K_e = \frac{K_0}{K_0 + (1 - K_0)e^{-R\delta/D}}, \quad (2)$$

where R is the growth rate, D is the solute diffusion coefficient, and δ is the diffusion boundary layer thickness. After applying the ultrasonic field, the acoustic streaming affected the natural convection mode in the traditional casting process. The convective heat transfer efficiency in the melt was enhanced, which increased the moving speed of

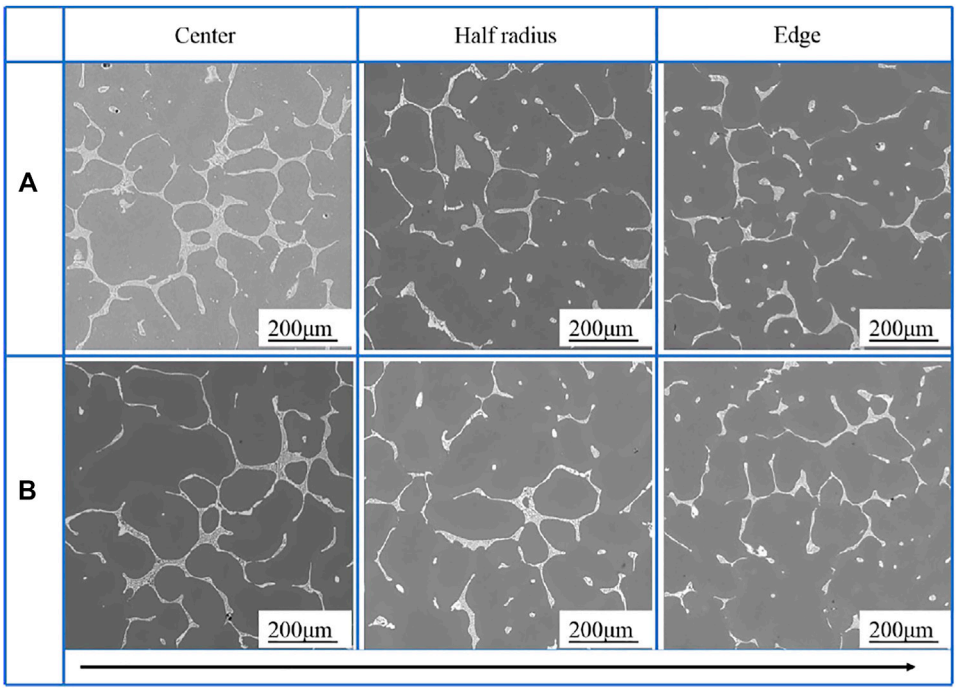

FIGURE 8 | The SEM images of the two ingots treated with **(A)** TSU and **(B)** DSU.

the solidification interface and reduced $e^{-R\delta/D}$. Therefore, the effective solute partition coefficient was increased (Aziz, 1982). The TSU of ultrasonic technology, ultrasonic melt convection heat transfer effect, was stronger than in the DSU during the process of casting. At the same time, the speed of collapsed cavitation bubbles was significantly promoted with the increase in the ultrasonic sound source number. Cu atoms were more uniformly diffused and distributed under the effect of the shock wave and the micro jet produced in the cavitation bubble collapsing process, reducing the degree of segregation. Moreover, it can be seen from **Figure 6** that under the action of TSU, the distribution of the sound pressure value in the sound pressure field was more evenly and significantly higher than that under the action of DSU. It further proved that TSU can reduce the macro-segregation of Cu content better than DSU. So the TSU technology for Cu segregation rate control effect was appropriate (Wang et al., 2013; Kotadia and Das, 2015).

Microstructure of the Al_2Cu Phase

The representative SEM images of the center, half radius, and edge of the two ingots are shown in **Figures 8A,B**. It can be seen from EDS results that the second phase is mainly Al_2Cu, which is consistent with the previous literature (Zhang et al., 2019c). The pictures show that the area of the Al_2Cu phase gradually decreased from the center to the edge, and the Al_2Cu phase was a cementite network structure. Moreover, compared with the DSU-treated ingot, the area of Al_2Cu at each position of the TSU-treated ingot was relatively smaller.

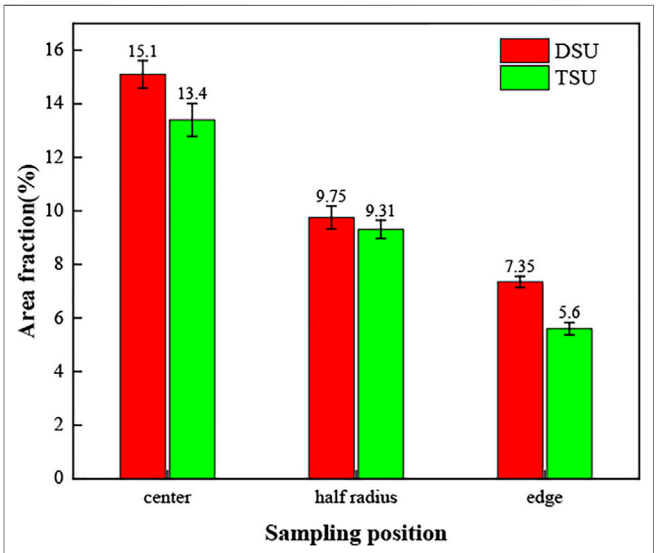

FIGURE 9 | Area fraction of the Al_2Cu phase.

IPP 6 software was used to calculate the area fraction of the Al_2Cu phase. As shown in **Figure 9**, the area fraction of the second phase of both ingots gradually decreased from the center to the edge. It was up to 15.1 and 13.4% in the center of two ingots. In contrast, this value decreased by 11.3%. The area fraction of the Al_2Cu phase at the edge was 7.35 and 5.6%, showing a significant reduction of 23.8%.

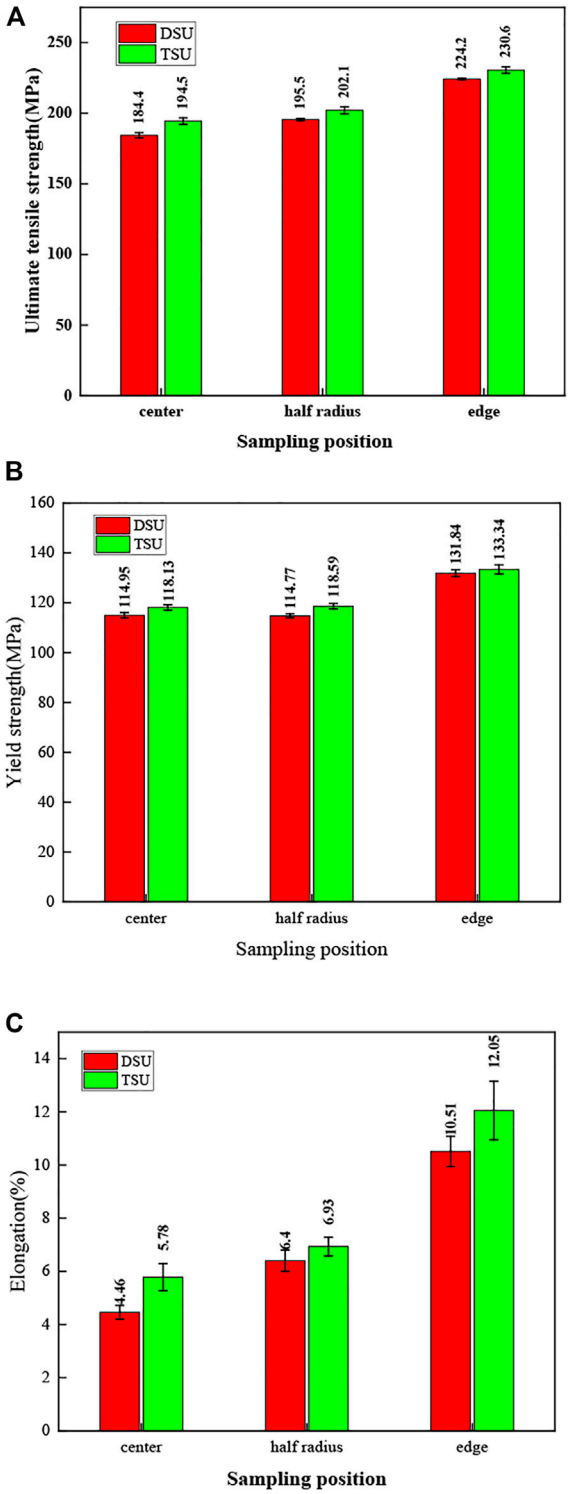

FIGURE 10 | Mechanical properties: **(A)** TS, **(B)** YS, and **(C)** EL determined at different positions.

The refinement of the Al_2Cu phase was attributed to the following mechanism: 1) forced stirring and homogenization of acoustic streaming. The Cu atom was more uniformly distributed in the whole ingot, which reduced the formation of thick Al_2Cu (Kotadia et al., 2017; Kamal Babu et al., 2018); 2) ultrasonic cavitation was helpful for fragmentation and nucleation, accelerating the heat transfer and cooling rates inside the melt and thus inhibiting the growth of Al_2Cu (Ruvalcaba et al., 2007; Zhang et al., 2019); and 3) the grain refinement effect of ultrasonic treatment. The interface energy decreased with the increasing area of grain boundaries. The Al_2Cu phase was more likely to nucleate at the grain boundary, which inhibited the growth of matrix crystals and reduced the continuity of the second phase (Zhang et al., 2019).

Mechanical Properties

Tensile strength (TS), yield strength (YS), and elongation (EL) of each sample are shown in **Figure 10**. Mechanical properties of the edge parts were better than those of the center and half-radius positions. The mechanical properties of the TSU-treated ingot at each location were better than those of the DSU-treated ingot specimens. After being treated with TSU, TS of the ingot increased by 5.5, 3.4, and 2.9%, respectively, and EL improved by 30, 8.3, and 14.7%, respectively. It indicates that the mechanical properties of ingots were significantly expanded by the high-energy ultrasonic. According to the Hall-Petch formula (Hansen, 2004),

$$\sigma_s = \sigma_0 + Kd^{-1/2}, \tag{3}$$

where σ_0 is the YS constant of the material, K is the slope of the straight line, and d is the grain size. It can be seen that the YS of the sample was negatively correlated with the grain size. According to Hansen, k can be taken as 0.14 MPa. Thus, as the grain size at the center decreased from 324.1 to 226.4 μm, σ_s increased by 1.09 MPa. The results showed that the σ_s increased to 3.18 MPa. Therefore, the improvement of the mechanical properties of the sample was not the only cause for grain refinement as the second phase Al_2Cu and ultrasonic fields also played an important role in the sample structure. The precipitation of the second phase was promoted by the application of ultrasonic fields so that more Al_2Cu phases were uniformly distributed in the matrix (Kotadia et al., 2017). Moreover, the interface energy and the bonding strength between the matrix and the second phase were evidently improved by the α-Al grains which were refined under ultrasonic treatment (Ruvalcaba et al., 2007; Ceschini et al., 2011). In general, the mechanical properties were effectively improved by the refined α-Al matrix and Al_2Cu phases (Wang et al., 2014; Zhang et al., 2019).

The fracture morphologies of the DSU-treated and TSU-treated ingots are shown in **Figures 11A,B,C,D**, respectively. As shown in **Figure 11**, two ingots' center parts had visible rough tearing edges, and the surface was covered with a thick bright white phase with a large fracture size. The fracture surface at the edges of the sample was reduced, and most of the fracture surfaces were densely distributed along the grain, with more dimples and smooth fracture planes. This indicates that the center part was prone to cause stress concentration due to the large area of the second coarse phase (Nadella et al.,

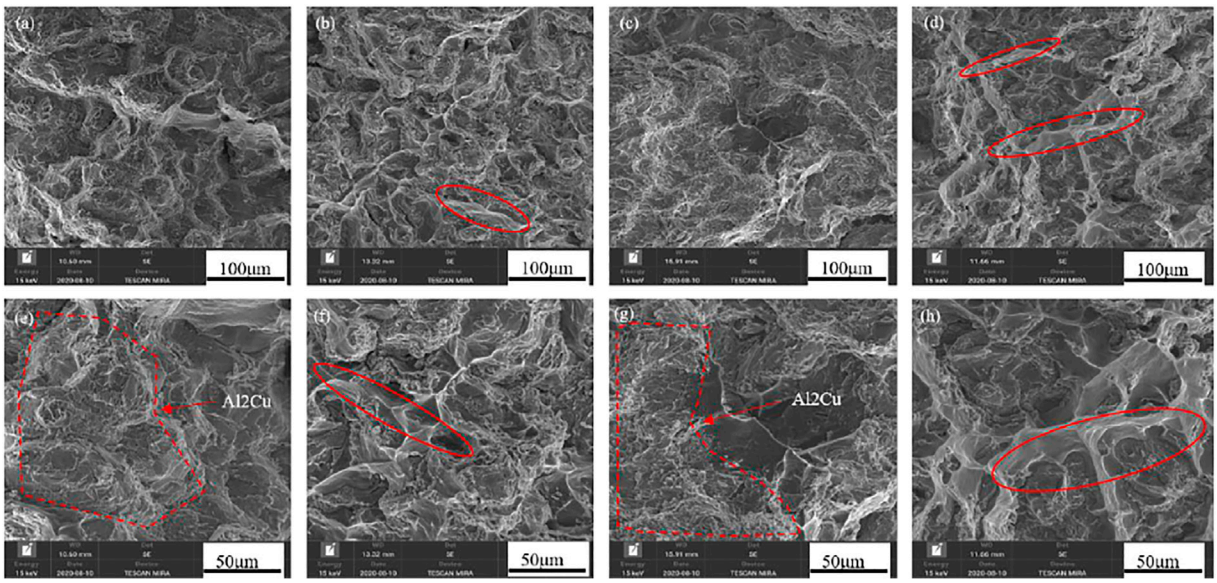

FIGURE 11 | Fracture morphology: **(A, E)** the center part, and **(B, F)** the edge part in the ingot with the TSU; **(C, G)** the center part, and **(D, H)** the edge part in the ingot with the DSU.

2008). At the edge, this phenomenon has been ameliorated considerably. The stress concentration on the grain boundary reduced, and the phenomenon of the fine grain strengthening was evident, which led to an improvement in the ingot's plasticity and effectively reduced the occurrence of cracks in the subsequent deformation of the large ingot (Jung et al., 2017; Chen et al., 2018; Moussa et al., 2018; Beets et al., 2019). Moreover, the edge specimen did not sacrifice plasticity. EL had also been greatly improved. This showed that grain refinement and the second phase–strengthening effect could simultaneously improve the strength and plasticity of the ingot, and the ability to resist the grain dislocation slip was increased in the process of deformation.

CONCLUSION

In this work, the differences in the α-Al grain size, macroscopic segregation, mechanical properties, and Al_2Cu phase in the α-Al matrix from 2219 aluminum alloy ingots were mainly investigated under the DSU and TSU processes. The main findings are listed as follows:

(1) The hydrogen content in the center and the half radius of an ingot treated with TSU was greatly decreased from 0.028 cm^3/100 g and 0.026 cm^3/100 g to 0.016 cm^3/100 g, respectively, and in the DSU-treated ingot from 0.012 cm^3/100 g to 0.015 cm^3/100 g, in the TSU-treated ingot.
(2) Under the TSU technology, the average grain sizes of the α-Al matrix at three representative locations were 234.1, 226.4, and 152.1 μm, respectively, which were 27.8, 22.1, and 12.7% less than that under the DSU technology. The grain sizes at the edges were greatly refined by water cooling, while the influence of power ultrasonic in this position was ignorable. Under the TSU, the macroscopic segregation rate of the ingot was relatively low, with a maximum deviation of 5.5%. But, the segregation rate was 7.7% under the DSU and exhibited a decrease of 28.6%. Moreover, the Cu atoms were more evenly distributed under the TSU.
(3) The center of the ingot was mainly composed of thick Al_2Cu phases and α-Al matrices. Additionally, the second phase was mostly distributed in a thick network. Under the TSU, the grain was refined in the edge. Meanwhile, the second phase Al_2Cu was narrowed and thinned, with an increasing discontinuity, and the grain was distributed in the shape of point and bone.
(4) The ultimate tensile strength, yield strength, and elongation of the ingot samples treated with TSU were higher than those processed with DSU. The mechanical properties were closely related to the grain size of the α-Al matrix and Al_2Cu phase. The α-Al refinement effect was better under TSU treatment, and the second phase Al_2Cu distribution was more uniform, which made the mechanical properties of the ingot better than those under the DSU.

DATA AVAILABILITY STATEMENT

The datasets presented in this study can be found in online repositories. The names of the repository/repositories and accession number(s) can be found in the article/Supplementary Material.

AUTHOR CONTRIBUTIONS

AL was responsible for writing the manuscript, drawing the icon of the experimental data, testing the experimental results, and consulting the data; RJ and ZL were responsible for the on-site guidance of the experiment and the revision of the article; RL was responsible for revising the article, analyzing the experimental results, and searching the literature; and YZ was responsible for guiding the revision and writing of the paper.

FUNDING

This work was supported by the National Natural Science Foundation of China (No. 51805549,52005517), Natural Science Foundation of the Hunan Province (No.2020JJ4703, No.2021JJ40774), and the Science and Technology Innovation Plan of the Hunan Province (No.2020RC 2002). This work was also supported by Xinjiang Join world Company Limited (No.738010042).

REFERENCES

Aziz, M. J. (1982). Model for Solute Redistribution during Rapid Solidification. *J. Appl. Phys.* 53, 1158–1168. doi:10.1063/1.329867

Beets, N., Cui, Y., Farkas, D., and Misra, A. (2019). Mechanical Response of a Bicontinuous Copper-Molybdenum Nano-Composite: Experiments and Simulations. *Acta Materialia* 178, 79–89. doi:10.1016/j.actamat.2019.07.045

Ceschini, L., Morri, A., Morri, A., and Pivetti, G. (2011). Predictive equations of the tensile properties based on alloy hardness and microstructure for an A356 gravity die cast cylinder head. *Mater. Des.* 32, 1367–1375. doi:10.1016/j.matdes.2010.09.014

Chen, X., Jia, Y., Liao, Q., Jia, W., Le, Q., Ning, S., et al. (2019). The Simultaneous Application of Variable Frequency Ultrasonic and Low Frequency Electromagnetic fields in Semi Continuous Casting of AZ80 Magnesium alloy. *J. Alloys Compd.* 774, 710–720. doi:10.1016/j.jallcom.2018.09.300

Chen, X., Ning, F., Hou, J., Le, Q., and Tang, Y. (2018). Dual-frequency Ultrasonic Treatment on Microstructure and Mechanical Properties of ZK60 Magnesium alloy. *Ultrason. Sonochem.* 40, 433–441. doi:10.1016/j.ultsonch.2017.07.027

Eskin, G. I., and Eskin, D. G. (2003). Production of Natural and Synthesized Aluminum-Based Composite Materials with the Aid of Ultrasonic (Cavitation) Treatment of the Melt. *Ultrason. Sonochem.* 10, 297–301. doi:10.1016/S1350-4177(02)00158-X

Eskin, G. I., and Eskin, D. G. (2014). *Ultrasonic Treatment of Light alloy Melts*. Boca Raton: CRC Press. doi:10.1201/b17270

Hansen, N. (2004). Hall-Petch Relation and Boundary Strengthening. *Scripta Materialia* 51, 801–806. doi:10.1016/j.scriptamat.2004.06.002

Jiang, R., Li, X., Chen, P., Li, R., and Zhang, X. (2014). Effect and Kinetic Mechanism of Ultrasonic Vibration on Solidification of 7050 Aluminum alloy. *AIP Adv.* 4, 077125. doi:10.1063/1.4891035

Jiang, R. P., and Li, X. Q. (2015). Investigation on the Mechanism of Grain Refinement in Aluminum Alloy Solidified under Ultrasonic Vibration. *Met. Mater. Int.* 21, 104–108. doi:10.1007/s12540-015-1012-x

Jung, J.-G., Lee, J.-M., Cho, Y.-H., and Yoon, W.-H. (2017). Combined Effects of Ultrasonic Melt Treatment, Si Addition and Solution Treatment on the Microstructure and Tensile Properties of Multicomponent Al Si Alloys. *J. Alloys Compd.* 693, 201–210. doi:10.1016/j.jallcom.2016.09.006

Kamal Babu, K., Panneerselvam, K., Sathiya, P., Haq, A. N., Sundarrajan, S., Mastanaiah, P., et al. (2018). Influences of Metastable θ″, θ′ and Stable θ Intermetallics Formed during Cryorolling and Friction Stir Welding Process on AA2219. *J. Alloys Compd.* 732, 624–629. doi:10.1016/j.jallcom.2017.10.212

Khosro Aghayani, M., and Niroumand, B. (2011). Effects of Ultrasonic Treatment on Microstructure and Tensile Strength of AZ91 Magnesium alloy. *J. Alloys Compd.* 509, 114–122. doi:10.1016/j.jallcom.2010.08.139

Kotadia, H. R., and Das, A. (2015). Modification of Solidification Microstructure in Hypo- and Hyper-Eutectic Al-Si Alloys under High-Intensity Ultrasonic Irradiation. *J. Alloys Compd.* 620, 1–4. doi:10.1016/j.jallcom.2014.09.089

Kotadia, H. R., Qian, M., Eskin, D. G., and Das, A. (2017). On the Microstructural Refinement in Commercial Purity Al and Al-10 Wt% Cu alloy under Ultrasonication during Solidification. *Mater. Des.* 132, 266–274. doi:10.1016/j.matdes.2017.06.065

Li, R., Liu, Z., Dong, F., Li, X., and Chen, P. (2016). Grain Refinement of a Large-Scale Al Alloy Casting by Introducing the Multiple Ultrasonic Generators during Solidification. *Metall. Mat Trans. A.* 47, 3790–3796. doi:10.1007/s11661-016-3576-6

Liew, P. J., Yan, J., and Kuriyagawa, T. (2014). Fabrication of Deep Micro-holes in Reaction-Bonded SiC by Ultrasonic Cavitation Assisted Micro-EDM. *Int. J. Machine Tools Manufacture* 76, 13–20. doi:10.1016/j.ijmachtools.2013.09.010

Liu, Y., Deng, C., Gong, B., and Bai, Y. (2019). Effects of Heterogeneity and Coarse Secondary Phases on Mechanical Properties of 7050-T7451 Aluminum alloy Friction Stir Welding Joint. *Mater. Sci. Eng. A* 764, 138223. doi:10.1016/j.msea.2019.138223

Liu, Z., Li, R., Jiang, R., Zhang, L., and Li, X. (2019). Scalable Ultrasound-Assisted Casting of Ultra-large 2219 Al Alloy Ingots. *Metall. Mat Trans. A.* 50, 1146–1152. doi:10.1007/s11661-018-5097-y

Ma, C., Chen, L., Cao, C., and Li, X. (2017). Nanoparticle-induced Unusual Melting and Solidification Behaviours of Metals. *Nat. Commun.* 8, 14178. doi:10.1038/ncomms14178

Moussa, M. E., Waly, M. A., and Amin, M. (2018). Effect of High Intensity Ultrasonic Treatment on Microstructural Modification and Hardness of a Nickel-Aluminum Bronze alloy. *J. Alloys Compd.* 741, 804–813. doi:10.1016/j.jallcom.2018.01.218

Nadella, R., Eskin, D. G., Du, Q., and Katgerman, L. (2008). Macrosegregation in Direct-Chill Casting of Aluminium Alloys. *Prog. Mater. Sci.* 53, 421–480. doi:10.1016/j.pmatsci.2007.10.001

Patel, B., Chaudhari, G. P., and Bhingole, P. P. (2012). Microstructural Evolution in Ultrasonicated AS41 Magnesium alloy. *Mater. Lett.* 66, 335–338. doi:10.1016/j.matlet.2011.08.113

Ruvalcaba, D., Mathiesen, R. H., Eskin, D. G., Arnberg, L., and Katgerman, L. (2007). *In Situ* observations of Dendritic Fragmentation Due to Local Solute-Enrichment during Directional Solidification of an Aluminum alloy. *Acta Materialia* 55, 4287–4292. doi:10.1016/j.actamat.2007.03.030

Sharma, V. M. J., Kumar, K. S., and Pathak, S. D. (2009). Effect of Microstructure and Strength on the Fracture Behavior of AA2219 alloy. *Mater. Sci. Eng. A* 502, 45–53. doi:10.1016/j.msea.2008.11.024

Tian, Y., Liu, Z., Li, X., Zhang, L., Li, R., Jiang, R., et al. (2018). The Cavitation Erosion of Ultrasonic Sonotrode during Large-Scale Metallic Casting: Experiment and Simulation. *Ultrason. Sonochem.* 43, 29–37. doi:10.1016/j.ultsonch.2017.12.053

Wang, F., Chiu, Y.-L., Eskin, D., Du, W., and Shearing, P. R. (2021). A Grain Refinement Mechanism of Cast Commercial Purity Aluminium by Vanadium. *Mater. Characterization* 181, 111468. doi:10.1016/j.matchar.2021.111468

Wang, F., Eskin, D., Connolley, T., and Mi, J. (2016). Effect of Ultrasonic Melt Treatment on the Refinement of Primary Al3Ti Intermetallic in an Al-0.4Ti alloy. *J. Cryst. Growth* 435, 24–30. doi:10.1016/j.jcrysgro.2015.11.034

Wang, F., Qiu, D., Liu, Z.-L., Taylor, J. A., Easton, M. A., and Zhang, M.-X. (2014). Crystallographic Study of Grain Refinement of Al by Nb Addition. *J. Appl. Cryst.* 47, 770–779. doi:10.1107/s1600576714004476

Wang, F., Qiu, D., Liu, Z.-L., Taylor, J. A., Easton, M. A., and Zhang, M.-X. (2013). The Grain Refinement Mechanism of Cast Aluminium by Zirconium. *Acta Materialia* 61, 5636–5645. doi:10.1016/j.actamat.2013.05.044

Wang, F., Tzanakis, I., Eskin, D., Mi, J., and Connolley, T. (2017). *In Situ* observation of Ultrasonic Cavitation-Induced Fragmentation of the Primary Crystals Formed in Al Alloys. *Ultrason. Sonochem.* 39, 66–76. doi:10.1016/j.ultsonch.2017.03.057

Wang, H., Yi, Y., and Huang, S. (2016). Influence of Pre-deformation and Subsequent Ageing on the Hardening Behavior and Microstructure of 2219 Aluminum alloy Forgings. *J. Alloys Compd.* 685, 941–948. doi:10.1016/j.jallcom.2016.06.111

Xu, H., Han, Q., and Meek, T. T. (2008). Effects of Ultrasonic Vibration on Degassing of Aluminum Alloys. *Mater. Sci. Eng. A* 473, 96–104. doi:10.1016/j.msea.2007.04.040

Zhang, L., Eskin, D. G., and Katgerman, L. (2011). Influence of Ultrasonic Melt Treatment on the Formation of Primary Intermetallics and Related Grain Refinement in Aluminum Alloys. *J. Mater. Sci.* 46, 5252–5259. doi:10.1007/s10853-011-5463-2

Zhang, L., Li, R., Jiang, R., Zhang, L., and Li, X. (2019c). A Comparative Study on the Effect of Four-Source Ultrasonic Power on the Microstructure and Mechanical Properties of Large-Scale 2219 Aluminum Ingots. *Jom* 71, 2063–2071. doi:10.1007/s11837-019-03459-y

Zhang, L., Li, X., Jiang, R., Li, R., and Zhang, L. (2019a). Effect of Ultrasonic Treatment on Grain Structure, Eutectic Phase and Mechanical Properties of an Al–6.2 Wt% Cu Alloy. *Met. Mater. Int.* 27 (5), 1282–1295. doi:10.1007/s12540-019-00508-8

Zhang, L., Li, X., Li, R., Jiang, R., and Zhang, L. (2019b). Effects of High-Intensity Ultrasound on the Microstructures and Mechanical Properties of Ultra-large 2219 Al alloy Ingot. *Mater. Sci. Eng. A* 763, 138154. doi:10.1016/j.msea.2019.138154

Zhang, Y., Li, R., Chen, P., Li, X., and Liu, Z. (2019). Microstructural Evolution of Al2Cu Phase and Mechanical Properties of the Large-Scale Al alloy Components under Different Consecutive Manufacturing Processes. *J. Alloys Compd.* 808, 151634. doi:10.1016/j.jallcom.2019.07.346

Conflict of Interest: The authors declare that the research was conducted in the absence of any commercial or financial relationships that could be construed as a potential conflict of interest.

Publisher's Note: All claims expressed in this article are solely those of the authors and do not necessarily represent those of their affiliated organizations, or those of the publisher, the editors, and the reviewers. Any product that may be evaluated in this article, or claim that may be made by its manufacturer, is not guaranteed or endorsed by the publisher.